Smart Drug Delivery through DNA/Magnetic Nanoparticle Gates

Eduardo Ruiz-Hernández, Alejandro Baeza, and María Vallet-Regí*

Departamento de Química Inorgánica y Bioinorgánica, Facultad de Farmacia, Universidad Complutense de Madrid, Plaza Ramón y Cajal s/n, 28040 Madrid, Spain, and Networking Research Center on Bioengineering, Biomaterials and Nanomedicine (CIBER-BBN), Spain

ABSTRACT Mesoporous silica nanoparticles can be modified to perform on-demand stimuli-responsive dosing of therapeutic molecules. The silica network was loaded with iron oxide superparamagnetic nanocrystals, providing the potential to perform targeting and magnetic resonance imaging. Single-stranded DNA was immobilized onto the material surface. The complementary DNA sequence was then attached to magnetic nanoparticles. The present work demonstrates that DNA/magnetic nanoparticle conjugates are able to cap the pores of the magnetic silica particles upon hybridization of both DNA strands. Progressive double-stranded DNA melting as a result of temperature increase gave rise to uncapping and the subsequent release of a mesopore-filled model drug, fluorescein. The reversibility of DNA linkage results in an "on−off" release mechanism. Moreover, the magnetic component of the whole system allows reaching hyperthermic temperatures (42−47 °C) under an alternating magnetic field. This feature leaves open the possibility of a remotely triggered drug delivery. Furthermore, due to its capacity to increase the temperature of the surrounding media, this multifunctional device could play an important role in the development of advanced drug delivery systems for thermochemotherapy against cancer.

KEYWORDS: mesoporous silica · magnetic nanoparticles · iron oxide · DNA · drug delivery · stimuli-responsive · hyperthermia

In many clinical situations, medication doses are oversized as a result of impaired drug absorption or tissue unspecific delivery.[1,2] This fact becomes a critical issue in the field of oncology, where the ratio of risk−benefit associated with chemotherapeutic agents is frequently unmanageable. The development of nano- and microparticles as drug delivery systems has emerged as one of the most groundbreaking biomedical applications. Advances associated with nanosystem preparation in the world of nanomedicine have challenged the scientists to develop smart functional materials able to address unmet drug release conditions.[3−6]

A special concern with regards to drug delivery systems deals with the design of carriers capable of selectively releasing their payloads at target sites in the body. Magnetic nanoparticles represent a promising alternative for active drug targeting since they can be concentrated and held in position by means of an external field.[7] Moreover, their superparamagnetic behavior provides multifunctional effects such as controlled heating capability under an alternating magnetic field, which is suitable for hyperthermic treatment of cancer[8−11] as well as tumor-specific delivery of nanoparticles.[12] Additionally, they can be used in bioseparation applications, diagnosis as enhancing contrast agents in magnetic resonance imaging, cell separation, and detoxification of biological fluids.[13−16]

In addition to targeting performance, a selective and safe drug delivery device would display a stimuli-responsive behavior,[17] which should be tailored for on-demand dosing. The design of stimuli-responsive biomaterials where an external stimulus (*e.g.*, changes in pH, temperature, magnetic field, *etc.*) results in a change of properties and causes a controlled drug release remains a challenge. A proper nanodevice for on-demand drug delivery requires switchability, so that it is repeatedly activated after reaching the targeted cells or tissues.

Mesoporous silica materials[18] show attractive features, such as biocompatibility,[19] stable mesoporous structures, large surface areas, and tunable pore sizes and volumes, making them ideal for controlled delivery of drugs[20−23] or even proteins.[24−26] Previous reports on functional mesoporous silica nanomaterials describe several moieties that could serve as gating devices, triggering the release of guest molecules by different external stimuli such as chemicals,[27−31] pH,[32−34] temperature,[35] redox reactions,[36−38] enzymes,[39] and photoirradiation.[40−46] Magnetic mesoporous silica has also been organically modified[47] to provide both a hosting matrix for the therapeutic cargo and a means for controlling further release.

In other respects, superparamagnetic nanocrystals covalently linked to a nucleic acid strand have been reported to capture external electromagnetic energy and break the hydrogen bonding pattern with its complementary strand.[48] Furthermore, the use

*Address correspondence to vallet@farm.ucm.es.

Received for review October 28, 2010 and accepted January 10, 2011.

Published online January 20, 2011
10.1021/nn1029229

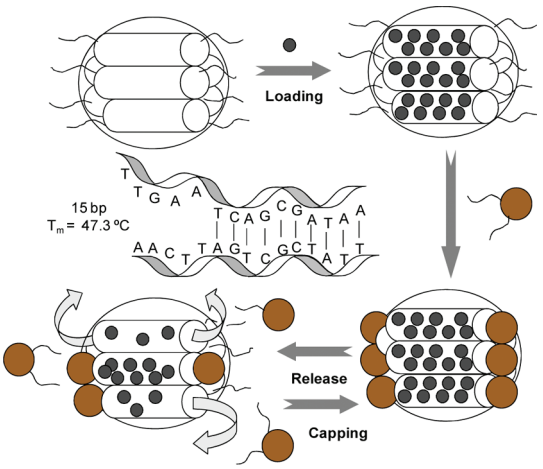

Scheme 1. Reversible magnetic nanogates drive drug release from magnetic mesoporous silica particles through DNA hybridization/dehybridization.

of a nucleic acid duplex as a heat labile and reversible system incorporates the additional feature of temperature tunability through changes in chain length, variations in G/C content, or even the size and surface density of oligonucleotides attached to the nanocrystals.[49] In this text, we describe the integration of superparamagnetic nanoparticles with a magnetic mesoporous silica network through thermosensitive oligonucleotide linkage. As a result, the natural ability of DNA molecules to reversibly hybridize is applied as a gatekeeping mechanism for drug dosing.

In our system, oligonucleotide-modified mesoporous silica, encapsulating iron oxide superparamagnetic nanoparticles, is loaded with fluorescein and subsequently capped with magnetic nanocrystals functionalized with the complementary strand (Scheme 1). DNA duplex was selected to display a melting temperature of 47 °C, which corresponds to the upper limit of therapeutic magnetic hyperthermia. In this way, we assess the potential of this device to combine anticancer thermotherapy with triggered drug release under a single remotely controlled stimulus, which is the alternating magnetic field. Such synergistic effect represents a promising approach in combined treatments against solid tumors.

RESULTS AND DISCUSSION

Oligonucleotide Anchorage on Mesoporous Silica. Spherical γ-Fe_2O_3 (maghemite) nanoparticles were initially prepared according to a previously reported method.[50] The ferrofluid so-obtained was composed of magnetic nanoparticles with an average diameter of 5 nm, as estimated from transmission electron microscopy (TEM) images.[51] A panoramic view of the colloid after drying is shown in Figure 1a.

After that, the magnetic nuclei were reacted with aminopropyltriethoxysilane (APTES).[52] The resulting amino-functionalized nanoparticles were divided into two batches. One of them was employed to build the

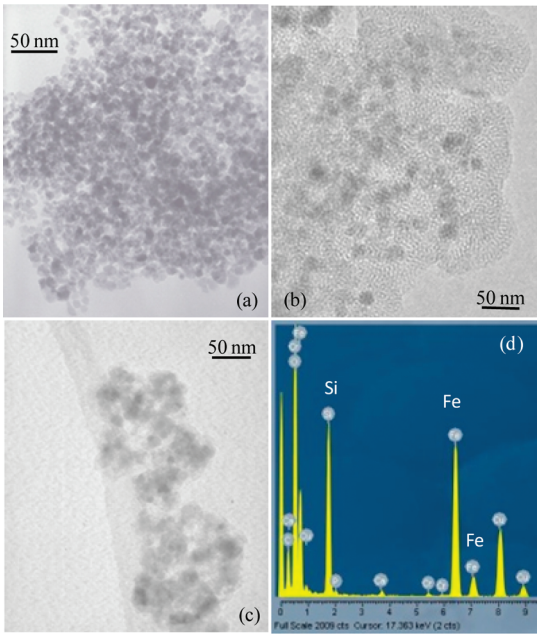

Figure 1. TEM micrographs of (a) γ-Fe_2O_3 magnetic nanoparticles, (b) magnetic mesoporous silica particles, (c) silica nanoparticles capped through DNA/magnetic nanoparticle gates, and (d) EDX analysis of the sample in (c).

capping system as described below. The second batch was added into the synthesis of the cetyltrimethylammonium bromide (CTAB)-templated mesoporous silica matrix, which is produced following a method described elsewhere.[53] Aminopropyl groups on the surface of the iron oxide cores cause a displacement in the isoelectric point of the bare maghemite colloid (data not shown). It is hypothesized that this effect gives rise to an enhanced interaction between the magnetic nanoparticles and the surfactant−silica hybrid mesostructure, as a result of the reduction in the density of negative electric charges at basic pH. Thus, the incorporation of the iron oxide into the silica matrix is facilitated. This method provides an effective means of integrating the as-synthesized magnetic cores into the mesoporous network.

Once the surfactant is removed, magnetic mesoporous particles (MMP) of 100 nm average hydrodynamic size, as measured by dynamic light scattering (DLS), are obtained. Nitrogen sorption isotherm (Figure 2a) of the composite material, displaying a characteristic adsorption step in the 0.2−0.4 relative pressure range, can be classified as type IV according to IUPAC. The absence of a hysteresis loop is characteristic of mesoporous systems with cylindrical pores open at both ends. The surface area of the particles is 776 $m^2 \cdot g^{-1}$, with a narrow pore size distribution centered at 2.5 nm, as shown in the inset. Figure 1b and Figure 3 display TEM and SEM observations, respectively, of mesoporous silica aggregates. In the former, the magnetic nuclei can be distinguished with a darker contrast in the micrograph.

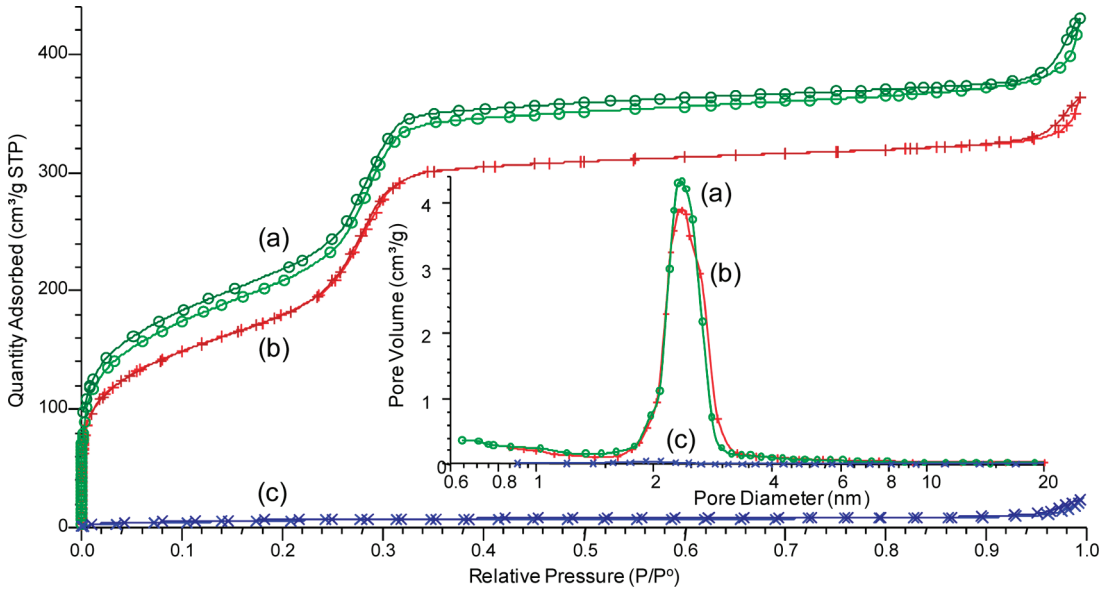

Figure 2. N_2 adsorption isotherms of (a) magnetic mesoporous particles (MMP), (b) amine-functionalized MMP, and (c) capped amine-functionalized MMP. Inset: corresponding pore size distributions.

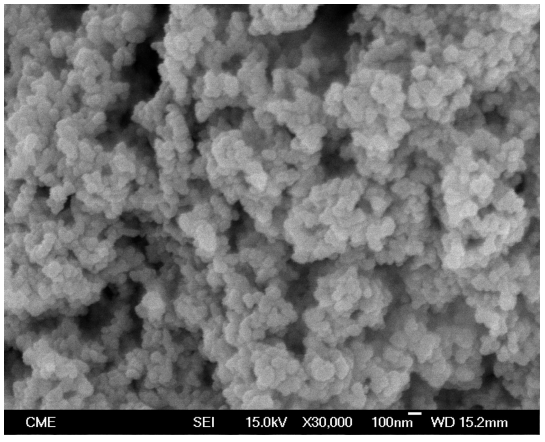

Figure 3. SEM micrograph of magnetic mesoporous silica particles (MMP).

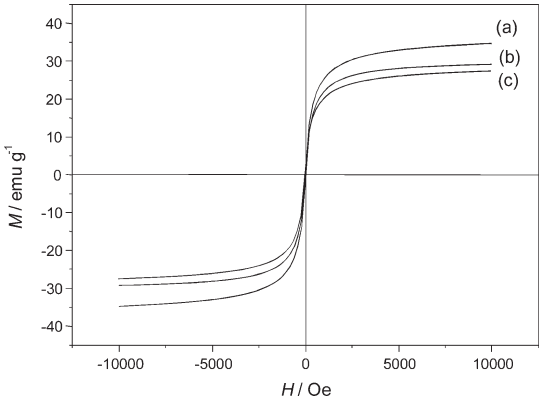

Figure 4. Vibrating sample magnetometry measurements of (a) nonfunctionalized, (b) thiol-functionalized, and (c) amine-functionalized magnetic mesoporous silica particles.

In order to provide a suitable surface for oligonucleotide attachment onto the magnetic silica particles, two different strategies were tested. The first approach required a thiol-functionalized surface, which was obtained through the reaction with mercaptopropyltriethoxysilane. In the second one, the material was reacted with APTES to get an aminated surface. Vibrating sample magnetometry of bare and functionalized particles demonstrates that superparamagnetism, characteristic of the incorporated magnetic cores,[51] is preserved in the process of encapsulation and chemical modification (Figure 4). None of these samples exhibit hysteresis in their magnetization curves. The saturation magnetization values, ranging from 28 to 35 emu·g^{-1}, are consistent with a 45−56% wt content of maghemite in the particles.

The oligonucleotide sequence (5′-thiolC6-TTATC-GCTGATTCAA) to be anchored to the mesoporous network surface was selected to present a melting temperature of 47 °C. This temperature coincides with the upper limit of cancer hyperthermia temperature range, as stated above. For the DNA grafting onto the thiol-modified particles, a disulfide bridge was formed with the 15 bp oligonucleotide *via* a thiol/disulfide exchange reaction under basic conditions.[54] This method presents the advantage of its simplicity, but the total amount of grafted DNA, indirectly calculated by UV−vis spectroscopy measurements of free DNA remaining in the reaction media, was disappointing (5%). In our second approach, a sulfo-SMCC cross-linker[55] was first linked to the aminated mesoporous silica surface, followed by reaction with the 5′-thiol-modified oligonucleotide (Scheme 2). The average amount of anchored DNA in this case was 60%. Given that a higher degree of functionalization would lead to a more efficient mesopore capping, the latter approach was followed.

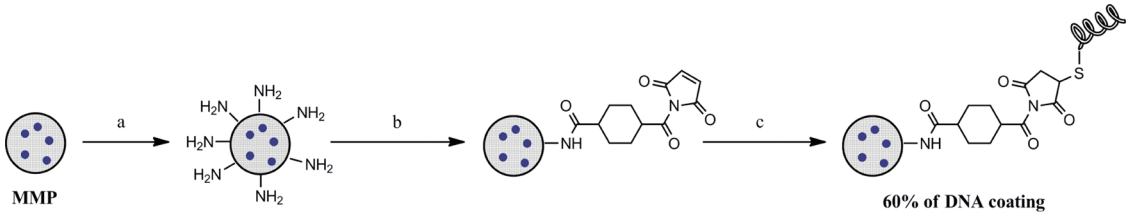

Scheme 2. Synthetic strategy for DNA grafting onto the surface of mesoporous silica.

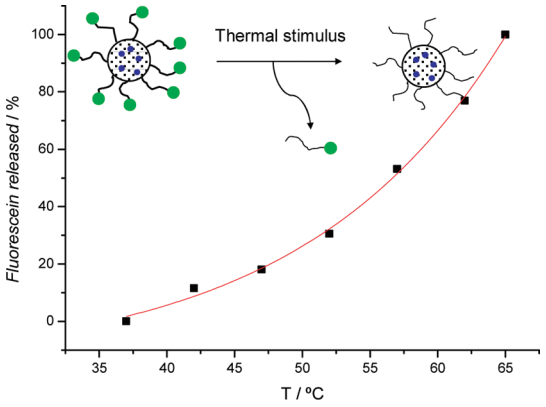

Figure 5. Temperature-dependent release of fluorescein-tagged oligonucleotide from the surface of DNA-conjugated MMP. Data have been normalized to the maximum level of fluorescein released in the experiment.

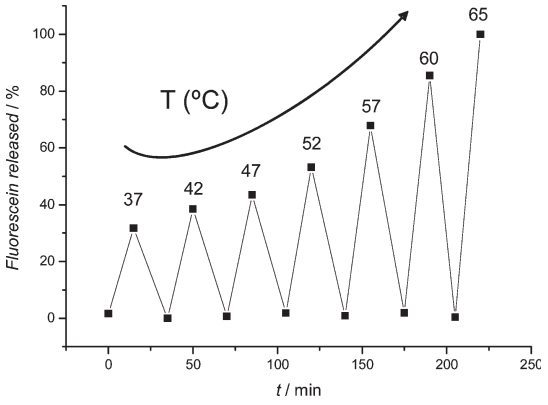

Figure 6. Fluorescein-labeled oligonucleotide release profile from mesoporous silica particles as a function of time–temperature in a dehybridization/rehybridization sequence. Data have been normalized to the maximum level of fluorescein released in the experiment.

The functionalization step in the mesoporous matrix is expected to affect the textural properties.[23] In our case, a slight reduction in surface area (674 $m^2 \cdot g^{-1}$), as well as pore volume (from 0.67 $cm^3 \cdot g^{-1}$, in the case of MMP, to 0.56 $cm^3 \cdot g^{-1}$) and mesopore diameter (2.3 nm), was found after functionalizing with amine groups. In spite of this decrease in the adsorption capacity, the nitrogen sorption isotherm of these amino-modified particles is essentially similar to that of MMP (Figure 2b).

Thermosensitive Behavior of the Oligonucleotides Immobilized onto Silica Particles. With the aim to determine the performance of the oligonucleotides attached to the mesoporous silica surface in response to changes in temperature, the complementary oligonucleotides labeled with a fluorescent probe ([Flc]TTGAATCAGCGATAA) were hybridized with the particles. A certain amount of the conjugated material was placed in an incubator shaker at different temperature set points, until the level of fluorescence in the supernatant remained constant, as measured by spectrofluorimetry. Figure 5 shows the maximum amount of fluorescein-tagged oligonucleotide released at each temperature, indicating the degree of DNA melting. As previously mentioned, the oligonucleotide chain length and the G/C proportion in the composition, among some other parameters, would define the temperature profile.

In order to assess the on–off behavior of the system, after maintaining the temperature for 15 min, the particles were cooled to room temperature (20 °C). Interestingly, everytime the thermal stimulus was removed, the fluorescein-labeled oligonucleotides were retained again within the mesoporous silica, and fluorescein detection in the supernatant was close to zero (Figure 6). This fact ensures a reversible mechanism through DNA rehybridization.

Complementary Oligonucleotides/Iron Oxide Nanoparticle Assembly for Mesopore Gating. The other batch of the amino-functionalized magnetic nuclei was conjugated with the complementary 5′-thiol-modified oligonucleotide (5′-thiolC6-TTGAATCAGCGATAA) through the sulfo-SMCC cross-linker. After that, a dispersion of these nanoparticles was added to oligonucleotide-conjugated MMP to allow for DNA hybridization. TEM observations aided by energy-dispersive X-ray spectroscopy (EDX) of hybridized particles (MMP-Fe complex) show that the characteristic contrast of mesoporous silica is indistinguishable in this sample, and only aggregates of magnetic nuclei are displayed (Figure 1c). However, punctual EDX analysis indicates overlapping Si and Fe element detection (Figure 1d), from which an effective coupling between iron oxide cores and silica particles could be inferred.

DLS measurements helped to determine both the proper amount of maghemite nanoparticles and their corresponding surface density of oligonucleotides to obtain uniform MMP-Fe complexes, while avoiding aggregation between mesoporous silica particles. Figure 7 displays the monomodal distribution of MMP-Fe complex (Figure 7a), centered on 200 nm hydrodynamic diameter, which is consistent with the presence of

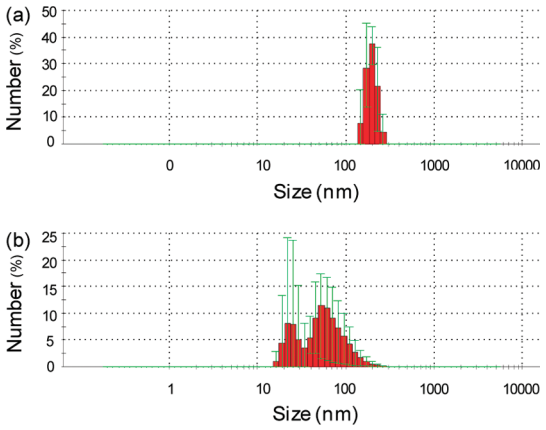

Figure 7. Hydrodynamic size distribution profiles of (a) capped mesoporous particles, and (b) a mixture of mesoporous silica particles with the magnetic caps without DNA linkage.

uniform self-assembled aggregates of oligonucleotide-modified magnetic nuclei attached to the surface of the mesoporous silica particles. A more irregular profile indicating the presence of unspecific aggregates is found when amino-modified MMP and iron oxide nanoparticles are just mixed, without DNA linking between both species (Figure 7b).

The ability of the oligonucleotide-conjugated magnetic nanocrystals to integrate with the mesoporous network and block the pore entrance is assessed by nitrogen sorption porosimetry. The isotherm corresponding to the MMP-Fe complex (Figure 2c) shows a drastic reduction in the adsorption properties. Values of surface area (23 $m^2 \cdot g^{-1}$) and pore volume (0.036 $cm^3 \cdot g^{-1}$) are in accordance with severe pore blocking in the structure. For comparison purposes, textural analysis of the mixture of equal amounts of amino-modified MMP and iron oxide nanoparticles was also performed (Supporting Information). Mesoporous features (S_{BET} = 402 $m^2 \cdot g^{-1}$, pore volume = 0.32 $cm^3 \cdot g^{-1}$, pore diameter = 2.4 nm) found in this sample suggest no assembly of both materials in the absence of oligonucleotide linkage.

In order to test the stimuli-responsive behavior of the MMP-Fe complex, fluorescein was employed as an easily traceable drug model in release experiments. The mesoporous particles were loaded with fluorescein prior to complementary oligonucleotide hybridization. Drug release was monitored with increasing temperatures along the time of assay, measuring the total amount of fluorescein accumulated in the supernatant. The mixture of fluorescein-loaded amino-modified MMP and iron oxide nanoparticles was used as control. As presented in Figure 8a, on the one hand, the fluorescein release profile from the capped system follows an exponential behavior, which is temperature-dependent, and resembles that obtained in the previously referred experiments with fluorescein-labeled oligonucleotides (Figures 5 and 6). This fact

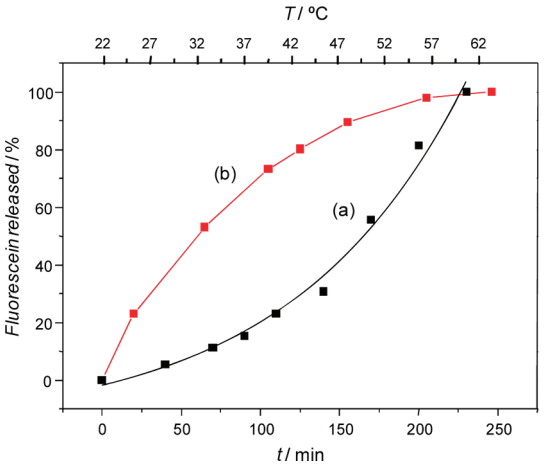

Figure 8. Fluorescein-loaded capped mesoporous delivery pattern (a), in comparison with the uncapped material (b). Data have been normalized to the maximum level of fluorescein released in the experiment.

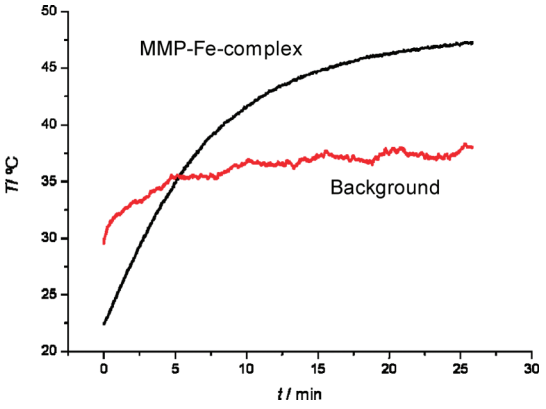

Figure 9. Hyperthermia assay on capped magnetic mesoporous silica under an alternating magnetic field of 24 $kA \cdot m^{-1}$ and 100 kHz.

suggests the 15 bp double helix uncapping as the drug delivery triggering mechanism. On the other hand, the control shows a typical release pattern associated with mesoporous matrices without capping,[23] irrespective of increasing temperatures (Figure 8b), where the drug is just diffused to the outer media.

The presence of magnetic species both inside the mesoporous network and on the surface of the MMP-Fe complex ensures the potential of the material to reach hyperthermia temperature range by using little amounts of the sample. In our experimental hyperthermic setup,[56] the fluorescein-loaded particles were exposed to an alternating magnetic field of 24 $kA \cdot m^{-1}$ and 100 kHz inside a thermostatic chamber at 37 °C. The particles are able to heat the environment to hyperthermia level after several minutes under the influence of the magnetic field (Figure 9), which is maintained until temperature stabilization of the medium (47 °C). When this time had elapsed, fluorescein released was in the same range as the amount liberated under the previously assayed thermal stimulus.

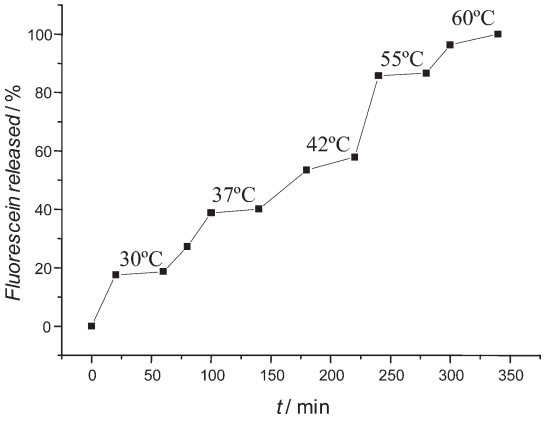

Figure 10. Temperature-responsive release curve of DNA/magnetic nanoparticle capped complex (MMP-Fe complex).

Eventually, the suitability of the DNA/magnetic nanoparticle conjugates to act as reversible gatekeepers for the mesoporous silica particles was examined. For this purpose, a certain amount of fluorescein-loaded MMP-Fe complex was placed in an incubation shaker with increasing temperatures and 40 min holding time at each point (Figure 10). Measurements of the total amount of fluorescein accumulated in the supernatant were acquired both once the set point was reached and after the holding time. The staircase profile of this release curve shows that fluorescein delivery is triggered when the temperature rises, while it is slowed on temperature stabilization. This "on−off" behavior reveals the MMP-Fe complex as a potential on-demand drug delivery system.

CONCLUSION

A stimuli-responsive controlled release material based on superparamagnetic mesoporous silica particles is presented. Iron oxide nanoparticles are suggested as caps for the porous matrix through a double helix DNA strand self-assembly. Guest molecules, such as fluorescein, can be encapsulated and further released under direct heating or the influence of an alternating magnetic field. The device combines the potential to perform"on−off" drug release with the capacity to increase the temperature of the surrounding media. Therefore, we envision that this material could play an important role in the development of advanced drug delivery systems for thermochemotherapy against cancer.

METHODS

Preparation of the Ferrofluid. The co-precipitation of Fe(II) (42.5 mL of 1.5 M HCl, 7.83 g of $FeCl_2 \cdot 4H_2O$) and Fe(III) (875 mL, 21.51 g of $FeCl_3 \cdot 6H_2O$) chlorides (molar ratio 1:2) with ammonia (75 mL, 30% wt) at pH 9.5 was carried out according to the Massart method,[50,57] yielding nanometric magnetite (Fe_3O_4). Following dispersion in 2 M HNO_3, the particles were oxidized to maghemite (γ-Fe_2O_3) by the addition of iron nitrate (150 mL, 20.41 g of $Fe(NO_3)_3 \cdot 9H_2O$) and heating at 90 °C for 30 min. After that, the product was washed with acetone several times and finally dispersed in water/HNO_3 to a concentration of 103 mg·mL^{-1}. The ferrofluid so-obtained was composed of magnetic nanoparticles with an average hydrodynamic diameter of 8 nm at pH 2.5, as measured by dynamic light scattering. The slight discrepancy between this result and the size estimated by TEM observations could be explained by the contribution of surface-bound water to the hydrodynamic diameter.[58] The isoelectric point of the resulting ferrofluid occurs at neutral pH (pH 7.1), as derived from ζ-potential results. Magnetic measurements from this ferrofluid are characteristic of a superparamagnetic material since no hysteresis loop is displayed in the magnetization curve, and saturation magnetization is equal to 58 emu·g^{-1} (62 emu·g^{-1} for the dry powdered nanoparticles). BET surface area of the dry powdered sample measured by nitrogen adsorption analysis was 140 m^2·g^{-1}.

Coating with Aminopropyltriethoxysilane (APTES). Aminopropyl groups were grafted onto γ-Fe_2O_3 nanoparticles following the well-known Stöber method.[59] In a typical synthesis, 22.8 mL of the ferrofluid was dispersed in 64 mL of deionized water with 10 drops of ammonia. After homogenizing, 242 mL of absolute ethanol and 16 mL of ammonia were added, and the mixture was exposed to sonication. APTES (12.85 μL) was dropped 20 min later, and sonication was then continued for 4 h. Finally, ammonia and ethanol were removed under reduced pressure.

Functionalized Magnetic Nanoparticles Encapsulation into Mesoporous Silica. APTES-modified maghemite nanoparticles were incorporated into mesoporous silica matrices employing a cationic surfactant, cetyltrimethylammonium bromide (CTAB), as structure-directing agent in basic pH conditions. This procedure is presented in the literature as the modified Stöber method.[53] In our experiment, 1.94 g of CTAB was dissolved in EtOH/NH_4OH/H_2O (molar ratio 1:0.8:2.5) with 24 mL of functionalized ferrofluid. The mixture was stirred for 15 min before tetraethylorthosilicate (4 mL) was added. After 2 h of additional vigorous stirring, the precipitate was centrifuged and washed with deionized water. In order to remove the template, the dried powder was heated to 425 at 5 °C min^{-1} in air and calcined for 3 h.

Chemical Modification of Mesoporous Silica Surface. A certain amount of template-free mesoporous material was degassed under vacuum at 90 °C for 72 h. Then, 100 mg was reacted with 1.34 mmol APTES in toluene. The whole reacting system together with the mesoporous material was purged with N_2 gas before the addition of APTES, so inert atmosphere was achieved within the system. Reactions were performed under reflux conditions for 16 h, and the products were filtered and washed with toluene. Amine-functionalized magnetic mesoporous silica was dried under vacuum at 90 °C for 72 h.

Oligonucleotide Immobilization. Dithio-DL-threitol (DTT), 0.1 M in 170 mM PBS buffer (pH 8.0), was used to ensure full reactivity of thiol-modified oligonucleotides. Before immobilization, all oligonucleotides (20 nmol) were suspended in 100 μL of DTT solution for 2 h. G-25 Sephadex columns (GE Healthcare) were then used for purifying the reduced thiolated products.

DNA coupling to amine-functionalized material was carried out by means of sulfosuccinimidyl 4-*N*-maleimidomethyl cyclohexane-1-carboxylate (sulfo-SMCC) as a cross-linker. Particles (10 mg) were first reacted with sulfo-SMCC for 2 h in 0.1 M PBS buffer, 0.2 M NaCl, pH 7.2. After removing the supernatant and washing to remove excess cross-linker, DNA was added and reacted overnight. The sequence attached to γ-Fe_2O_3-loaded mesoporous silica particles was 5′-thiolC6-TTATCGCTGATTCAA,

and the complementary sequence (5′-thiolC6-TTGAATCAG-CGATAA) was conjugated to functionalized magnetic nanoparticles. The melting temperature for these oligonucleotides is 47.3 °C, according to the manufacturer (Sigma). The DNA-immobilized nanoparticles were then washed three times in 10 mM Tris-HCl, 150 mM NaCl, and 0.05% Tween 20 buffer (pH 7.5). The amount of attached DNA was estimated by subtracting DNA accumulated in the supernatant and washing solutions from total DNA, measured by UV−vis spectrometry. The level of DNA functionalization per particle was purposely lowered in aminopropyl-grafted magnetic nanoparticles to avoid MMP aggregation. Finally, DNA conjugates were dispersed in a buffer of 20 mM Tris-HCl, 37.5 mM $MgCl_2$ (pH 8.0) for subsequent hybridization.

DNA Hybridization. As a proof of concept for the reversible hybridization/dehybridization mechanism of the selected DNA sequence, the complementary oligonucleotide described above, tagged with a fluorescein probe ([Flc]TTGAATCAGCGATAA), was hybridized with DNA-conjugated MMP. Both species were mixed in an orbital shaker at 120 rpm for 1 h.

In the case of the system with the gating mechanism, pore loading was performed during the DNA hybridization process. DNA-tagged magnetic nanoparticles were assembled in the same way after loading the MMP matrices with 1.2 M fluorescein in the hybridization buffer for 3 h. The product, denoted as MMP-Fe complex, was intensively washed to remove physisorbed fluorescein.

Fluorescein Release Assays. In order to investigate the release kinetics of fluorescein-labeled MMP and fluorescein-loaded MMP-Fe complex, as a function of both temperature and time, 10 mg of the material was redispersed in 2 mL of 0.1 M PBS, pH 7.2. Temperature changes were produced in an Infors-HT Ecotron incubator shaker. The alternating magnetic field at 24 $kA \cdot m^{-1}$ and 100 kHz was applied within a thermostatic chamber at 37 °C by means of a Celes AC function generator. Variations of temperature were monitored by Luxtron fluoroptic probes inside and outside the liquid.

Acknowledgment. This work was supported by the Spanish CICYT through project MAT2008-00736 and the CAM through project S2009MAT-1472. CIBER-BBN is an initiative funded by the VI National R&D&i Plan 2008-2011, Iniciativa Ingenio 2010, Consolider Program, CIBER Actions and financed by the Instituto de Salud Carlos III with assistance from the European Regional Development Fund. Technical assistance from Microscopy Center-UCM and M. Maicas (ISOM-UPM) is acknowledged. In memory of Prof. Victor S. Y. Lin and Prof. Rafael Suau.

Supporting Information Available: Reagents, characterization techniques, calculation procedures, nitrogen sorption isotherms of the mixture of amino-modified MMP and amine-functionalized iron oxide nanoparticles (Figure S1a), and amine-functionalized iron oxide nanoparticles (Figure S1b). This material is available free of charge *via* the Internet at http://pubs.acs.org.

REFERENCES AND NOTES

1. Verstappen, C. C. P.; Heimans, J. J.; Hoekman, K.; Postma, T. J. Neurotoxic Complications of Chemotherapy in Patients with Cancer: Clinical Signs and Optimal Management. *Drugs* **2003,** *63*, 1549–1563.
2. Gupta, P. K. Drug Targeting in Cancer Chemotherapy: A Clinical Perspective. *J. Pharm. Sci.* **1990,** *79*, 949–962.
3. Ferrari, M. Cancer Nanotechnology: Opportunities and Challenges. *Nat. Rev.* **2005,** 161–171.
4. Jotterand, F. Nanomedicine: How It Could Reshape Clinical Practice. *Nanomedicine* **2007,** 401–405.
5. Moghimi, S. M.; Hunter, A. C.; Murray, J. C. Nanomedicine: Current Status and Future Prospects. *FASEB J.* **2005,** 311–330.
6. Farokhzad, O. C.; Langer, R. Nanomedicine: Developing Smarter Therapeutic and Diagnostic Modalities. *Adv. Drug Delivery Rev.* **2006,** 1456–1459.
7. Lübbe, A.; Bergemann, C.; Brock, J.; McClure, D. G. Physiological Aspects in Magnetic Drug-Targeting. *J. Magn. Magn. Mater.* **1999,** 149–155.
8. Hildebrandt, B.; Wust, P.; Ahlers, O.; Dieing, A.; Sreenivasa, G.; Kerner, T.; Felix, R.; Riess, H. The Cellular and Molecular Basis of Hyperthermia. *Crit. Rev. Oncol. Hematol.* **2002,** 33–56.
9. Overgaard, J. Effect of Hyperthermia on Malignant Cells *In Vivo*: A Review and a Hypothesis. *Cancer* **1977,** 2637–2646.
10. Sharma, R.; Chen, C. J. Newer Nanoparticles in Hyperthermia Treatment and Thermometry. *J. Nanopart. Res.* **2009,** 671–689.
11. Jordan, A.; Scholz, R.; Maier-Hauff, K.; Johannsen, M.; Wust, P.; Nadobny, J.; Schirra, H.; Schmidt, H.; Deger, S.; Loening, S.; *et al.* Presentation of a New Magnetic Field Therapy System for the Treatment of Human Solid Tumors with Magnetic Fluid Hyperthermia. *J. Magn. Magn. Mater.* **2001,** 118–126.
12. Kong, G.; Braun, R. D.; Dewhirst, M. W. Hyperthermia Enables Tumor-Specific Nanoparticle Delivery: Effect of Particle Size. *Cancer Res.* **2000,** *60*, 4440–4445.
13. Gupta, A. K.; Gupta, M. Synthesis and Surface Engineering of Iron Oxide Nanoparticles for Biomedical Applications. *Biomaterials* **2005,** 3995–4021.
14. Liong, M.; Lu, J.; Kovochich, M.; Xia, T.; Ruehm, S. G.; Nel, A. E.; Tamanoi, F.; Zink, J. I. Multifunctional Inorganic Nanoparticles for Imaging, Targeting, and Drug Delivery. *ACS Nano* **2008,** *2*, 889–896.
15. Molday, R. S.; Mackenzie, D. Immunospecific Ferromagnetic Iron-Dextran Reagents for the Labeling and Magnetic Separation of Cells. *J. Immunol. Methods* **1982,** 353–367.
16. Cheon, J.; Lee, J. H. Synergistically Integrated Nanoparticles as Multimodal Probes for Nanobiotechnology. *Acc. Chem. Res.* **2008,** 1630–1640.
17. Yoshida, M.; Lahann, J. Smart Nanomaterials. *ACS Nano* **2008,** *2*, 1101–1107.
18. Trewyn, B. G.; Slowing, I. I.; Giri, S.; Chen, H.-T.; Lin, V. S. Y. Synthesis and Functionalization of a Mesoporous Silica Nanoparticle Based on the Sol−Gel Process and Applications in Controlled Release. *Acc. Chem. Res.* **2007,** *40*, 846–853.
19. Lu, J. L.; Liong, M.; Li, Z.; Zink, J. I.; Tamanoi, F. Biocompatibility, and Drug-Delivery Efficiency of Mesoporous Silica Nanoparticles for Cancer Therapy in Animals. *Small* **2010,** *6*, 1794–1805.
20. Vallet-Regi, M.; Ramila, A.; del Real, R. P.; Perez-Pariente, J. A New Property of MCM-41: Drug Delivery System. *Chem. Mater.* **2001,** *13*, 308–311.
21. Muñoz, B.; Ramila, A.; Perez-Pariente, J.; Diaz, I.; Vallet-Regi, M. MCM-41 Organic Modification as Drug Delivery Rate Regulator. *Chem. Mater.* **2003,** *15*, 500–503.
22. Trewyn, B. G.; Whitman, C. M.; Lin, V. S. Y. Morphological Control of Room-Temperature Ionic Liquid Templated Mesoporous Silica Nanoparticles for Controlled Release of Antibacterial Agents. *Nano Lett.* **2004,** *4*, 2139–2143.
23. Balas, F.; Manzano, M.; Horcajada, P.; Vallet-Regi, M. Confinement and Controlled Release of Bisphosphonates on Ordered Mesoporous Silica-Based Materials. *J. Am. Chem. Soc.* **2006,** *128*, 8116–8117.
24. Han, Y.-J.; Stucky, G. D.; Butler, A. Mesoporous Silicate Sequestration and Release of Proteins. *J. Am. Chem. Soc.* **1999,** *121*, 9897–9898.
25. Yiu, H. H. P.; Wright, P. A.; Botting, N. P. Enzyme Immobilisation Using Siliceous Mesoporous Molecular Sieves. *Microporous Mesoporous Mater.* **2001,** *44−45*, 763–768.
26. Song, S. W.; Hidajat, K.; Kawi, S. Functionalized SBA-15 Materials as Carriers for Controlled Drug Delivery: Influence of Surface Properties on Matrix-Drug Interactions. *Langmuir* **2005,** *21*, 9568–9575.
27. Lai, C.-Y.; Trewyn, B. G.; Jeftinija, D. M.; Jeftinija, K.; Xu, S.; Jeftinija, S.; Lin, V. S. Y. A Mesoporous Silica Nanosphere-Based Carrier System with Chemically Removable CdS Nanoparticle Caps for Stimuli-Responsive Controlled Release of Neurotransmitters and Drug Molecules. *J. Am. Chem. Soc.* **2003,** *125*, 4451–4459.

28. Radu, D. R.; Lai, C.-Y.; Jeftinija, K.; Rowe, E. W.; Jeftinija, S.; Lin, V. S. Y. Fine-Tuning the Degree of Organic Functionalization of Mesoporous Silica Nanosphere Materials *via* an Interfacially Designed Co-condensation Method. *J. Am. Chem. Soc.* **2004,** *126*, 13216–13217.
29. Nguyen, T. D.; Leung, K. C. F.; Liong, M.; Pentecost, C. D.; Stoddart, J. F.; Zink, J. I. Construction of a pH-Driven Supramolecular Nanovalve. *Org. Lett.* **2006,** *8*, 3363–3366.
30. Leung, K. C. F.; Nguyen, T. D.; Stoddart, J. F.; Zink, J. I. Supramolecular Nanovalves Controlled by Proton Abstraction and Competitive Binding. *Chem. Mater.* **2006,** *18*, 5919–5928.
31. Slowing, I. I.; Trewyn, B. G.; Lin, V. S. Y. Mesoporous Silica Nanoparticles for Intracellular Delivery of Membrane-Impermeable Proteins. *J. Am. Chem. Soc.* **2007,** *129*, 8845–8849.
32. Park, C.; Oh, K.; Lee, S. C.; Kim, C. Controlled Release of Guest Molecules from Mesoporous Silica Particles Based on a pH-Responsive Polypseudorotaxane Motif. *Angew. Chem., Int. Ed.* **2007,** *46*, 1455–1457.
33. Casasus, R.; Climent, E.; Marcos, M. D.; Martinez-Manez, R.; Sancenon, F.; Soto, J.; Amoros, P.; Cano, J.; Ruiz, E. Dual Aperture Control on pH- and Anion-Driven Supramolecular Nanoscopic Hybrid Gate-like Ensembles. *J. Am. Chem. Soc.* **2008,** *130*, 1903–1917.
34. Angelos, S.; Yang, Y.-W.; Patel, K.; Stoddart, J. F.; Zink, J. I. pH-Responsive Supramolecular Nanovalves Based on Cucurbit[6]uril Pseudorotaxanes. *Angew. Chem., Int. Ed.* **2008,** *47*, 2222–2226.
35. Fu, Q.; Rao, G. V. R.; Ista, L. K.; Wu, Y.; Andrzejewski, B. P.; Sklar, L. A.; Ward, T. L.; Lopez, G. P. Control of Molecular Transport Through Stimuli-Responsive Ordered Mesoporous Materials. *Adv. Mater.* **2003,** *15*, 1262–1266.
36. Hernandez, R.; Tseng, H.-R.; Wong, J. W.; Stoddart, J. F.; Zink, J. I. An Operational Supramolecular Nanovalve. *J. Am. Chem. Soc.* **2004,** *126*, 3370–3371.
37. Nguyen, T. D.; Tseng, H.-R.; Celestre, P. C.; Flood, A. H.; Liu, Y.; Stoddart, J. F.; Zink, J. I. A Reversible Molecular Valve. *Proc. Natl. Acad. Sci. U.S.A.* **2005,** *102*, 10029–10034.
38. Nguyen, T. D.; Liu, Y.; Saha, S.; Leung, K. C. F.; Stoddart, J. F.; Zink, J. I. Design and Optimization of Molecular Nanovalves Based on Redox-Switchable Bistable Rotaxanes. *J. Am. Chem. Soc.* **2007,** *129*, 626–634.
39. Patel, K.; Angelos, S.; Dichtel, W. R.; Coskun, A.; Yang, Y.-W.; Zink, J. I.; Stoddart, J. F. Enzyme-Responsive Snap-Top Covered Silica Nanocontainers. *J. Am. Chem. Soc.* **2008,** *130*, 2382–2383.
40. Mal, N. K.; Fujiwara, M.; Tanaka, Y. Photocontrolled Reversible Release of Guest Molecules from Coumarin-Modified Mesoporous Silica. *Nature* **2003,** *421*, 350–353.
41. Angelos, S.; Choi, E.; Voegtle, F.; De Cola, L.; Zink, J. I. Photo-Driven Expulsion of Molecules from Mesostructure Silica Nanoparticles. *J. Phys. Chem. C* **2007,** *111*, 6589–6592.
42. Nguyen, T. D.; Leung, K. C. F.; Liong, M.; Liu, Y.; Stoddart, F.; Zink, J. I. Versatile Supramolecular Nanovalves Reconfigured for Light Activation. *Adv. Funct. Mater.* **2007,** *17*, 2101–2110.
43. Johansson, E.; Choi, E.; Angelos, S.; Liong, M.; Zink, J. I. Light-Activated Functional Mesostructured Silica. *J. Sol–Gel Sci. Technol.* **2008,** *46*, 313–322.
44. Lu, J.; Choi, E.; Tamanoi, F.; Zink, J. I. Light-Activated Nanoimpeller-Controlled Drug Release in Cancer Cells. *Small* **2008,** *4*, 421–426.
45. Park, C.; Lee, K.; Kim, C. Photoresponsive Cyclodextrin-Covered Nanocontainers and Their Sol–Gel Transition Induced by Molecular Recognition. *Angew. Chem., Int. Ed.* **2009,** *48*, 1275–1278.
46. Vivero-Escoto, J. L.; Slowing, I. I.; Wu, C.-W.; Lin, V. S. Y. Photoinduced Intracellular Controlled Release Drug Delivery in Human Cells by Gold-Capped Mesoporous Silica Nanosphere. *J. Am. Chem. Soc.* **2009,** *131*, 3462–3463.
47. Giri, S.; Trewyn, B. G.; Stellmaker, M. P.; Lin, V. S. Y. Magnetic Nanoparticle-Capped Mesoporous Silica Nanorod-Based Stimuli-Responsive Controlled Release Delivery System. *Angew. Chem., Int. Ed.* **2005,** *44*, 5038–5044.
48. Derfus, A. M.; Maltzahn, G.; Harris, T. J.; Duza, T.; Vecchio, K. S.; Ruoslahti, E.; Bhatia, S. N. Remotely Triggered Release from Magnetic Nanoparticles. *Adv. Mater.* **2007,** *19*, 3932–3936.
49. Jin, R.; Wu, G.; Li, Z.; Mirkin, C. A.; Schatz, G. C. What Controls the Melting Properties of DNA-Linked Gold Nanoparticle Assemblies? *J. Am. Chem. Soc.* **2003,** *125*, 1643–1654.
50. Ruiz-Hernández, E.; López-Noriega, A.; Arcos, D.; Izquierdo-Barba, I.; Terasaki, O.; Vallet-Regí, M. Aerosol-Assisted Synthesis of Magnetic Mesoporous Silica Spheres for Drug Targeting. *Chem. Mater.* **2007,** *19*, 3455–3463.
51. Ruiz-Hernández, E.; López-Noriega, A.; Arcos, D.; Vallet-Regí, M. Mesoporous Magnetic Microspheres for Drug Targeting. *Solid State Sci.* **2008,** *10*, 421–426.
52. Bruce, I. J.; Sen, T. Surface Modification of Magnetic Nanoparticles with Alkoxysilanes and Their Application in Magnetic Bioseparations. *Langmuir* **2005,** *21*, 7029–7035.
53. Grün, M.; Lauer, I.; Unger, K. K. The Synthesis of Micrometer- and Submicrometer-Size Spheres of Ordered Mesoporous Oxide MCM-41. *Adv. Mater.* **1997,** *9*, 254–257.
54. Hilliard, L. R.; Zhao, X.; Tan, W. Immobilization of Oligonucleotides onto Silica Nanoparticles for DNA Hybridization Studies. *Anal. Chim. Acta* **2002,** *470*, 51–56.
55. Zhang, D.; Carr, D. J.; Alocilja, E. C. Fluorescent Bio-Barcode DNA Assay for the Detection of Salmonella Enterica Serovar Enteritidis. *Biosens. Bioelectron.* **2009,** *24*, 1377–1381.
56. Martín-Saavedra, F. M.; Ruiz-Hernández, E.; Boré, A.; Arcos, D.; Vallet-Regí, M.; Vilaboa, N. Magnetic Mesoporous Silica Spheres for Hyperthermia Therapy. *Acta Biomater.* **2010,** *6*, 4522–4531.
57. Massart, R. Preparation of Aqueous Magnetic Fluid in Alkaline and Acidic Media. *IEEE Trans. Magn.* **1981,** *17*, 1247–1248.
58. Nath, N.; Chilkoti, A. Label-Free Biosensing by Surface Plasmon Resonance of Nanoparticles on Glass: Optimization of Nanoparticle Size. *Anal. Chem.* **2004,** *76*, 5370–5378.
59. Stober, W.; Fink, A.; Bohn, E. Controlled Growth of Monodisperse Silica Spheres in the Micron Size Range. *J. Colloid Interface Sci.* **1968,** *26*, 62–69.